

Fission Fragment Yields Of $^{235}\text{U}(n_{th}, f)$ Evaluated By The CCONE Code System

Futoshi Minato^{1,2,3,*} and Osamu Iwamoto³

¹*Department of Physics, Kyushu University, Fukuoka 819-0395, Japan*

²*RIKEN Nishina Center for Accelerator-Based Science, Wako, Saitama 351-0198, Japan*

³*Nuclear Data Center, Japan Atomic Energy Agency, Tokai, Ibaraki 319-1195, Japan*

(Dated: April 30, 2024)

Fission fragment yield evaluations are one of the important nuclear data studies. Fission accompanies various physical observables such as prompt fission neutron, prompt fission gamma, and delayed-neutrons. When evaluating fission fragment yields, a study including correlations among those observables is essentially required. However, fission fragment yield data in the past JENDL libraries have been made by focusing only on experimental fragment yields, decay heats, and delayed neutron yields, and they have not been expanded into a wider range of fission observables. This is because the evaluation method adopted in the JENDL libraries could not study fission fragment yields and particle emissions from fragments simultaneously. To solve this problem, a calculation system with CCONE code is newly developed to estimate not only independent and cumulative fission fragment yields but also prompt fission neutron, prompt fission gamma, decay heats, and delayed-neutrons simultaneously. This system enables us to study a correlation between various fission observables. To determine lots of parameters in this system efficiently, a Gaussian process and a least square fitting are adopted. We tested the calculation system through a thermal neutron-induced fission on ^{235}U . In this paper, we demonstrate the performance of the parameter search method and show that experimental fission fragment yield data and other observables resulting from fission are reproduced well by the new calculation system.

I. INTRODUCTION

Distributions of fission fragments resulted from neutron-induced fission are one of the key data for developments of next-generation nuclear reactors and disposals of spent nuclear fuels. Accurate data of fission fragment yields are also required to monitor active reactors with reactor neutrinos [1]. Evaluated data of fission fragment yields are currently available in several nuclear data library such as Japanese Evaluated Nuclear Data Library (JENDL), Evaluated Nuclear Data File (ENDF), and Joint Evaluated Fission and Fusion (JEFF).

Recently, world-wide activities that evaluate new fission fragment yields based on recent knowledge on nuclear physics gains the momentum [2]. The movements are attributed from the background that discrepancies from experimental data are obtained for fission observables such as independent fission fragment yields (IFY), and spectra and multiplicities of prompt fission neutron (PFN) and prompt fission γ -rays (PFG) when calculating them with evaluated data of fission fragment yields. The origin of this problems is simply due to that conventional approaches of fission fragment yield evaluations adopted in JENDL, ENDF, and JEFF have not respected all observables resulted from fission in the evaluations. One of the typical examples is an overestimation of delayed-neutron yields in JENDL-4.0 calculated with a summation method of the fission product yield and decay data [3]. Although this problem was drastically mitigated in the latest version of JENDL, JENDL-5 [4], the

fission fragment yield data are still evaluated independently from PFN, PFG, and so on. To provide versatile fission fragment yield data, it is required to comprehensively consider various observables resulted from fission besides its fragment yields.

Neutron-induced fission is a complicated dynamics that involves energy dissipation, many deformation degrees of freedom, fluctuations along fission path, and so on. To fully understand them, microscopic theoretical models that consider nuclear correlations among them are becoming a powerful tool. However, those approaches still do not reach a satisfactory level for practical applications for nuclear data evaluations. Recent macroscopic approaches for fission dynamics based on a Langevin models show a good agreement with experimental data of pre-neutron fission fragment yields rather than microscopic models [5–7]. However, those approaches also fail to reproduce pre-neutron fission fragment yields and total kinetic energy (TKE) distributions simultaneously, which become crucial to calculate particle evaporation from fragments, at a low incident neutron energy. For these reasons, at least for pre-neutron fission fragment yields and TKE data, a phenomenological approach is still the most reliable if experimental data enough to adjust the parameters are available. Once we obtain pre-neutron fission fragment yields and TKE data, we can calculate various fission observables with a particle evaporation model.

We recently developed a new system of fission fragment yield evaluation using the Comprehensive Code for Nuclear data Evaluation (CCONE) [8]. By using a phenomenologically determined pre-neutron fission fragment and TKE data, it calculates not only independent and cumulative fission yields, but also various ob-

* E-mail: minato.futoshi.009@m.kyushu-u.ac.jp

servables resulting from fission using with decay data and the Hauser-Feshbach statistical model that describes particle evaporation from compound states. The basic idea has already been applied in some studies using with BeoH code [9–11], FIFRELIN code [12, 13], and FREYA [14, 15]. The characteristic point of our system is a new feature in the parameter search. Since fission calculations involves a lot of parameters, it is hard to determine them without much time cost. To overcome this issue, we used an approach combining a Bayesian optimization with Gaussian process (hereafter, we simply call "GP") and a generalized least squares (GLS) methods. Multiplying the advantages of GP and GLS, an appropriate parameter set can be sought rather efficiently. We tested our system by a thermal neutron-induced fission on ^{235}U . Sect. II describes the framework to evaluate the fission fragment yields with the newly developed CCONE system. Sect. III demonstrates the result of calculations and discuss the difference from JENDL-5. Sect. V summarize this work and give our perspectives.

II. METHODOLOGY

The calculation of fission fragment yield of our system with CCONE is separated to four parts. Figure 1 illustrates each part schematically. Part (A) and (B) in Fig. 1 are the neutron-nucleus reaction and the formation of compound nucleus, respectively. The calculation of these parts is carried out with a coupled-channel optical model, distorted-wave born approximation, and two-component exciton model that are already included in the former CCONE [8]. The detail of the calculation is described in Refs. [8, 16], and we do not go into the details in this paper. The newly implemented modules in the present CCONE are part (C) and (D) that are particle evaporations from pre-neutron fission fragments and β decays of post-neutron fission fragments toward stable nuclei, respectively. The particle evaporation process in part (C) is studied within a Hauser-Feshbach statistical model implemented in CCONE, while the β -decay process in part (D) is calculated with a Batemann approach code [17] and the evaluated decay data of JENDL-5 [4]. Pre-neutron mass yields are approximated by a sum of five Gaussians and charge distributions are estimated by the Z_p model [18] with parameter modifications. Excitation energies of fission fragments are calculated by an assumption of anisothermal model [19]. In the following sections, we demonstrate the present approaches for part (C) and (D) in detail.

A. Pre-neutron mass yields and TKE distributions

When a fission channel is energetically open, CCONE reads data of pre-neutron fission mass yields and TKE defined as $Y(A)$ and $\text{TKE}(A)$, respectively. The same systematics as Refs. [9–11] are adopted for $Y(A)$ and

$\text{TKE}(A)$ in this work, in which $Y(A)$ is calculated with a sum of five Gaussians

$$Y(A) = G_0(A, E_{in}) + G_1(A, E_{in}) + G_2(A, E_{in}), \quad (1)$$

where

$$G_0(A, E_{in}) = \frac{W_0(E_{in})}{\sqrt{2\pi}\sigma(E_{in})} \exp\left(-\frac{(A - \mu_0(E_{in}))^2}{2\sigma_0^2(E_{in})}\right), \quad (2)$$

$$G_i(A, E_{in}) = \frac{W_i(E_{in})}{\sqrt{2\pi}\sigma(E_{in})} \left\{ \exp\left(-\frac{(A - \mu_i(E_{in}))^2}{2\sigma_i^2(E_{in})}\right) + \exp\left(-\frac{(A - (A_c - \mu_i(E_{in})))^2}{2\sigma_i^2(E_{in})}\right) \right\}, \quad (3)$$

for $i = 1, 2$ and TKE is estimated from

$$\text{TKE}(A_h) = (p_0 - p_1 A_h) \left(1 - p_2 \exp\left(-\frac{(A_h - \frac{A_c}{2})^2}{p_3}\right) \right) + \epsilon_{\text{TKE}}. \quad (4)$$

Here, W_i, σ_i ($i = 0, 1, 2$) and p_i ($i = 0, 1, 2, 3$) are the parameters determined so as to reproduce experimental data, and A_h and A_c are the mass of a heavy fragment and a compound nucleus, respectively. Incident neutron energy is set to be thermal neutron as $E_{in} = E_{\text{thermal}} = 0.0253$ eV. The last term ϵ_{TKE} in Eq. (4) is introduced so that the average value with fragment yields becomes equal to $\overline{\text{TKE}} = 171.1$ MeV, which is obtained from experimental data [20–22]. TKE of a fragment with mass A and atomic number Z is estimated by

$$\text{TKE}(A_l, Z_l) = \text{TKE}(A_h, Z_h) = \text{TKE}(A_h) \frac{Z_l Z_h}{N_{ZZ}(A_h)}, \quad (5)$$

where the normalization coefficient denoted as N_{ZZ} is defined as

$$N_{ZZ}(A_h) = \frac{\sum_{l,h} Z_l Z_h C(A_h, Z_h)}{\sum_{(l),h} C(A_h, Z_h)}. \quad (6)$$

Here, l, h take all possible fragment pairs with mass A_l and A_h and $C(A, Z)$ is the charge distributions described in Sect. II B. As introduced in Ref. [9], we also consider a fluctuation of TKE from Eq. (4) by considering a width parameter

$$\sigma_{\text{TKE}}(A_l) = \sigma_{\text{TKE}}(A_h) = s_0 - s_1 \exp\left[-s_2 \left(A_h - \frac{A_c}{2}\right)^2\right], \quad (7)$$

where s_i ($i = 0, 1, 2$) are the parameters. This work adopted the same parameters as Ref. [10] for those of the five Gaussians, p_i and s_i .

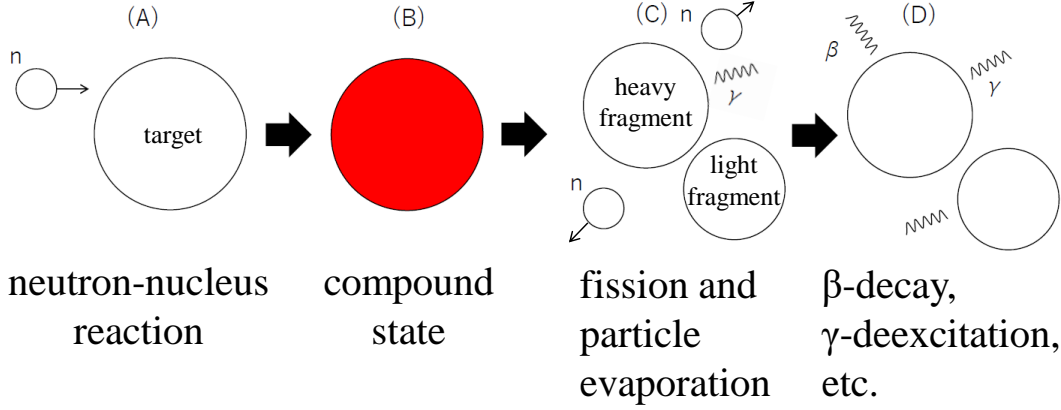


FIG. 1. Schematic picture of CCONE system of the fission fragment yield calculation.

B. Charge distributions

For charge distribution, we used Z_p model proposed by Wahl [18]. The pre-neutron fission fragment yields are represented by

$$Y(A, Z) = Y(A) \times C(A, Z), \quad (8)$$

where $C(A, Z)$ is given by

$$C(A, Z) = \int_{Z-0.5}^{Z+0.5} \frac{1}{\sqrt{2\pi}\sigma_p(A)} \exp\left(-\frac{(Z' - Z_p(A))^2}{2\sigma_p(A)^2}\right) dZ' \quad (9)$$

In this work, $Z_p(A)$ and $\sigma_p(A)$ are approximated by

$$Z_p(A) = Z_{p,\text{UCD}}(A) + \delta Z_p(A), \quad (10)$$

and

$$\sigma_p(A_l) = \sigma_p(236 - A_h) = 0.50 + \delta\sigma_p(A_l), \quad (11)$$

respectively, where $Z_{p,\text{UCD}}(A) \equiv \frac{Z_f}{A_f}A$ is the unchanged charge distribution, and $\delta Z_p(A)$ and $\delta\sigma_p(A)$ are free parameters to be determined by a parameter search method described later. Here, $Z_f = 92$ and $A_f = 236$ are the atomic and mass numbers of fissioning compound nucleus, that is ^{236}U . We consider $Z_p(A)$ in the range of $64 \leq A \leq 172$ as Wahl's evaluation [18], assuming $\delta Z_p(A_h) = -\delta Z_p(A_l)$ and $\delta\sigma_p(A_h) = \delta\sigma_p(A_l)$. We then have 55 free parameters for $\delta Z_p(A)$ and $\delta\sigma_p(A)$ from $A = 64$ to 118, respectively. However, the symmetric fission is rare event for the thermal neutron-induced fission on ^{235}U and $\delta Z_p(A = 118)$ is not uniquely determined within the least square fitting, so that we set $\delta Z_p(A = 118) = \delta\sigma_p(A = 118) = 0$ and excluded from the objects of parameter search.

Figure 2 shows $\delta Z_p(A) = Z_p - Z_{p,\text{UCD}}$ and $\sigma_p(A)$ of the evaluated data of England and Rider [23] and

Wahl [18]. Note that the evaluated data of England and Rider are for post-neutron fragment yields, while those of Wahl are for pre-neutron fragment yields. Therefore, the evaluated data of England Rider are systematically larger than those of Wahl and rotationally asymmetric around the point of $(A = 118, Z_p - Z_{p,\text{UCD}} = 0)$. In Wahl's evaluation, $Z_p(A)$ are determined by separating them into four parts, which are far-wing ($A_l \leq 70$), wing ($71 \leq A_l \leq 77$), peak ($78 \leq A_l \leq 105$), and near-symmetry regions ($106 \leq A_l \leq 118$). We can also observe in England and Rider evaluation that the $Z_p - Z_{p,\text{UCD}}$ have different behavior at $A_l < 78$, $78 \leq A_l < 96$, $96 \leq A_l < 104$, $104 \leq A_l < 108$, and $108 \leq A_l < 118$. In the following section, we demonstrate a performance of parameter search method by dividing $\delta Z_p(A)$ and $\delta\sigma_p(A)$ into $n = 5$ parts, and then discuss the result of full parameters.

C. Excitation energy distributions

Excitation distributions of fission fragment yields are estimated as follows. First, total excitation energy (TXE) is calculated by

$$\text{TXE} = E_{in} \frac{M_U}{M_U + M_n} + S_n + M_f - (M_l + M_h) - \text{TKE}, \quad (12)$$

where E_{in} is the incident neutron energy, S_n is neutron threshold of fissioning nucleus, and M_U , M_n , M_f , M_l , and M_h are the mass of ^{235}U , neutron, fissioning nucleus, light fragment, and heavy fragment, respectively. To sort TXE into two fission fragments, we use an anisothermal model [19]

$$R_T = \frac{T_l}{T_h} = \sqrt{\frac{a_h(U_h)U_l}{a_l(U_l)U_h}}, \quad (13)$$

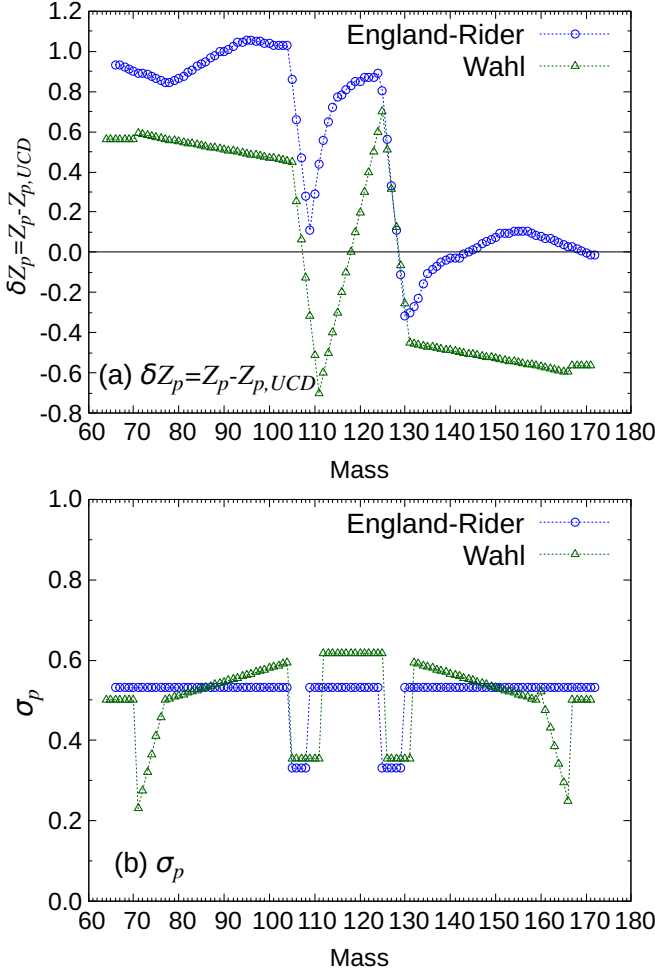


FIG. 2. (a) Differences between unchanged charge distribution and evaluated value of the most probable proton number Z_p of Wahl [18] without the odd-even effect. For comparison, those evaluated by England and Rider [23] in case of independent fission yields are shown. (b) Width parameter σ_p of charge distributions.

where $U_{l,h} = E_{l,h} - \Delta$, Δ being a correction energy attributed from pairing correlations [24]. The function $a_{l,h}(U_{l,h})$ is given by

$$a_{l,h}(U_{l,h}) = f_a a_{l,h}^* \left(1 + E_{sh;l,h} \frac{1 - e^{-\gamma U_{l,h}}}{U_{l,h}} \right), \quad (14)$$

where f_a , a^* , $E_{sh;l,h}$, γ are the scaling factor, the asymptotic level density parameter, the shell correction, and the shell damping factor, respectively. The mean excitation energies $E_{l,h}$ are estimated numerically from Eq. (13) with a condition of $E_l + E_h = \text{TXE}$. The excitation energy distributions are then estimated by [11]

$$F_{l,h}(E) = \frac{1}{\sqrt{2\pi}\sigma_{l,h}} \exp \left(-\frac{(E - E_{l,h})^2}{2\sigma_{l,h}^2} \right), \quad (15)$$

where the width is given by

$$\sigma_{l,h} = \frac{E_{l,h}}{\sqrt{E_l^2 + E_h^2}} \sigma_{\text{TKE}}, \quad (16)$$

where l and h in the above equations indicate light and heavy fragments respectively. As a consequence, fission fragment of mass A , atomic number Z , and excitation energy E is represented by

$$Y(A, Z, E) = Y(A, Z) \times F_{A,Z}(E) \quad (17)$$

In this work, a^* , E_{sh} , and γ in Eq. (14) are taken from Ref. [24], while the scaling factor f_a for fission fragments is sought by GP and GLS. It is ideally desirable to seek f_a for each fission fragments, however, we used the same f_a for all fission fragments because experimental data are limited to determine it accurately.

D. Odd-Even effects and Spin-Parity distributions

From experimental data, one can observe that fission fragment yields of nuclei with even-proton or even-neutron are larger than those of neighboring nuclei with odd-proton and odd-neutron. This effect is considered to be due to the pairing correlation; however its actual origin is not perfectly understood. To consider the odd-even effect to fission fragment yields in this work, we multiply $Y(A, Z, E)$ by a factor of f_Z (f_N) for even proton (neutron) number and divide for odd proton (neutron) number. After this correction, a renormalization is carried out to satisfy the condition:

$$\sum_{A,Z} \int Y(A, Z, E) dE = 2. \quad (18)$$

We assume equal distribution for odd and even parities. The fission fragment yields including the spin-parity distribution are given by [25]

$$Y(A, Z, E, J^\pi) = \frac{1}{2} \frac{J + 1/2}{2f_s^2 \sigma^2} \exp \left(\frac{(J + 1/2)^2}{2f_s^2 \sigma^2(U)} \right) Y(A, Z, E). \quad (19)$$

Here, the parameter f_s adjusts the magnitude of the spin cutoff parameter $\sigma(U)$, which is determined by the parameter search of this study.

E. Other input parameters

Transmission coefficients of nucleons are calculated by the optical potentials of Koning-Delaroché [26]. α , ^3He , ^3H and deuteron emissions from fission fragments are not considered in this work. Nuclear level schemes are taken from RIPL-3 [27]. For nuclear level densities, the Gilbert-Cameron method [25] with Mengoni-Nakajima parameter [24] is adopted. For γ strength functions, the enhanced generalized Lorentzian function [28] is used. Mass data are taken from the AME2020 [29].

III. SEEKING PARAMETERS AND EXPERIMENTAL DATA

In this section we explain the method to determine the parameters introduced in the previous section. Let us define $\mathbf{x} \equiv (\{\delta Z_p\}, \{\delta \sigma_p\}, R_T, f_Z, f_N, f_a, f_s)$. The number of parameters is 113 in total (δZ_p and $\delta \sigma_p$ have 54 parameters from $64 \leq A \leq 117$, respectively). The parameter search is carried out by finding \mathbf{x} that minimizes the objective function given by

$$O'(\mathbf{x}) = O(\mathbf{x}) + G(\mathbf{x}). \quad (20)$$

The first term of Eq. (20) is identical to χ^2 -distribution and defined as

$$O(\mathbf{x}) = \sum_i^{N_{\text{exp}}} \left| \frac{y_{\text{exp}}^{(i)} - y_{\text{calc}}^{(i)}(\mathbf{x})}{\delta y^{(i)}} \right|^2, \quad (21)$$

where $N_{\text{exp}} = 1055$ is the number of experimental data. The second term of Eq. (20) is introduced to regulate the range of parameters and given by

$$G(\mathbf{x}) = \exp \left(\sum_i^{N_{\text{par}}} \frac{|x^{(i)} - x_0^{(i)}|^2}{2(\Delta x_0^{(i)})^2} \right). \quad (22)$$

For x_0 and Δx_0 of $G(\mathbf{x})$ in Eq. (22), we used

$$(x_0, \Delta x_0) = \begin{cases} (0, 1.00) & \text{for } \Delta Z_p \\ (0, 0.25) & \text{for } \Delta \sigma_p \\ (1, 0.50) & \text{for } R_T \\ (1, 1.00) & \text{for } f_Z, f_N \\ (1, 0.50) & \text{for } f_a \\ (1, 4.00) & \text{for } f_s \end{cases} \quad (23)$$

As already introduced, a Bayesian optimization with the Gaussian process is adopted as one of the parameter search methods, where the Gaussian process is adopted to predicts $O'(\mathbf{x})$ of Eq. (20). The methodology is as follows. We first calculate $O'(\mathbf{x})$ with several different $\mathbf{x} = \mathbf{x}_{\text{inp}}$ determined randomly and store the result as the initial input data ($\{\mathbf{x}_{\text{inp}}, O'_{\text{inp}}\}$). Next, we predict the distribution of $O'(\mathbf{x}) = O'_{\text{pred}}(\mathbf{x})$ within the Gaussian process using the input data. From the predicted $O'_{\text{pred}}(\mathbf{x})$, we choose the most likely $\mathbf{x} = \mathbf{x}_{\text{new}}$ that gives the minimum $O'_{\text{pred}}(\mathbf{x})$ and it is added to the input data of $\{\mathbf{x}_{\text{inp}}, O'_{\text{inp}}\}$. Based on a Bayesian optimization, it is expected that one can find \mathbf{x} that gives minimum $O(\mathbf{x})$ by iterating this process many times. The formalism adopted in the present approach of GP is almost the same as [30]. The difference from Ref. [30] is the objective function of Eq. (20).

Another method to determine the most likely parameter set \mathbf{x} is GLS. Since outputs of the CCONE are generally non-linear against the input parameters, GLS is also carried out in an iterative way. New parameter set is determined by adding $\delta \mathbf{x}$ to old parameter set \mathbf{x}_{old} with a

regularization parameter μ ($0 < \mu \leq 1$) as

$$\mathbf{x}_{\text{new}} = \mathbf{x}_{\text{old}} + \mu \delta \mathbf{x}, \quad (24)$$

where $\delta \mathbf{x}$ is determined from GLS:

$$\delta \mathbf{x} = \mathbf{X} \mathbf{C}^T \left(\mathbf{V}^{-1} (\mathbf{y}_{\text{exp}} - \mathbf{y}_{\text{calc}}(\mathbf{x})) + \frac{(\mathbf{x}_0 - \mathbf{x})}{2\Delta \mathbf{x}_0^2} G(\mathbf{x}) \right). \quad (25)$$

The covariance matrix \mathbf{X} is defined as

$$\mathbf{X} = \left(\mathbf{C}^T \mathbf{V}^{-1} \mathbf{C} + \frac{1}{2\Delta \mathbf{x}_0^2} G(\mathbf{x}) \right)^{-1}, \quad (26)$$

where \mathbf{C} is the sensitivity matrix ($C_{ij} = \partial y_{\text{calc},i} / \partial x_j$) and \mathbf{V} ($V_{ij} = 1/(\delta y^{(i)})^2 \delta_{ij}$) is the covariance matrix of experimental data. In case of GLS, the initial \mathbf{x}_{old} are $\delta Z_p(A) = \delta \sigma_p(A) = 0, R_T = 1.0, f_Z = f_N = f_a = f_s = 1.0$, while they are determined from GP in case of GP+GLS. The regularization parameter μ is introduced so as to find the best parameter set smoothly and we give a different value of μ depending on the condition of $\delta \mathbf{x}$:

$$\mu = \begin{cases} 0.10 & (|\delta x^{(i)} / x_{\text{old}}^{(i)}| < 0.1) \\ 0.25 & (0.1 \leq |\delta x^{(i)} / x_{\text{old}}^{(i)}| < 1) \\ 0.40 & (1 \leq |\delta x^{(i)} / x_{\text{old}}^{(i)}| < 10) \\ 0.20 & (\text{other cases}). \end{cases} \quad (27)$$

Experimental data we used for the parameter search are listed in Table I. We adopted independent and cumulative fission yield data by Rudstam et al. [31], Tipnis et al. [32], prompt fission neutron yield data by Nishio et al. [33], Batenkov et al. [34], Vorobyev et al. [35], Boldeman et al. [36], Fraser et al. [37], Maslin et al. [38], and Göök et al. [39], averaged number of prompt γ multiplicities for light and heavy fragments by Pleasonton et al. [40], decay heat data by Akiyama et al. [41], Nguyen et al. [42], Dickens et al. [43], and delayed neutron yield data by Keepin et al. [44]. The total number of experimental data point is $N_{\text{exp}} = 1055$.

We have 54 free parameters for $Z_p(A)$ and $\sigma_p(A)$, respectively. If either $\delta Z_p(A)$ or $\delta \sigma_p(A)$ for a certain A is insensitive to the experimental data, we set $\delta Z_p(A) = 0$ or $\delta \sigma_p(A) = 0$ and exclude from the parameter fitting procedure. This case occurs especially for the far-wing part ($A \leq 70$ and $A \geq 166$) because of lack of experimental data in these regions.

IV. RESULT

A test calculation is carried out for a thermal neutron-induced fission on ^{235}U . The parameter search introduced in Sect. III has to be carried out to obtain independent fission fragment yields and fission observables reproducing experimental data. Before going to a parameter search for full set of $\mathbf{x} = (\{\delta Z_p\}, \{\delta \sigma_p\}, R_T, f_Z, f_N, f_a, f_s)$, we checked the performance of the parameter search method described in

TABLE I. Experimental data used for parameter search.

Type	Author	Ref.
IFY	Rudstam et al.	[31]
	Tipnis et al.	[32]
CFY	Rudstam et al.	[31]
	Tipnis et al.	[32]
PFN	Nishio et al.	[33]
	Batankov et al.	[34]
	Vorobyev et al.	[35]
	Boldeman et al.	[36]
	Fraser et al.	[37]
	Maslin et al.	[38]
	Göök et al.	[39]
Average number of PFG	Pleasanton et al.	[40]
Decay Heats after neutron irradiation	Akiyama et al.	[41]
	Nguyen et al.	[42]
	Dickens et al.	[43]
Delayed Neutrons after neutron irradiation	Keepin et al.	[44]
Total Delayed Neutron Yield	Keepin et al.	[44]

Sect. III by reducing the number of parameters. Assuming that $\delta Z_p(A)$ and $\delta \sigma_p(A)$ have a smooth dependence on A , we divide them into 5 parts, namely, $64 \leq A \leq 74$, $75 \leq A \leq 85$, $86 \leq A \leq 96$, $97 \leq A \leq 107$, and $108 \leq A \leq 117$. Finally we discuss the result of full parameter set of \mathbf{x} .

A. Test of parameter search with a reduced number of parameters

In this section, the result of the parameter search method for $\mathbf{x} = (\{\delta Z_p\}, \{\delta \sigma_p\}, R_T, f_Z, f_N, f_a, f_s)$ is discussed, where $\delta Z_p(A)$ and $\delta \sigma_p(A)$ ($64 \leq A \leq 117$) are divided into 5 parts. Thus, the number of parameters to be determined is 15 in total. We first carry out the parameter search by GP. The result of $O(\mathbf{x})$ is shown in Fig. 3, where the x -axis is the number of CCONE calculation, which is identical to the iteration time of GP. The minimum $O(\mathbf{x})$ that has been obtained in the past calculations is indicated by the triangle. The objective function oscillates around $O(\mathbf{x}) = 200$ and does not get converged even after 40 times of the calculations. We confirmed that $O(\mathbf{x})$ did not converge even if we increase the number of iteration up to 200. Analyzing the history of \mathbf{x} in this parameter search, GP tries various kinds of \mathbf{x} in the 15-dimension parameter space. In general, GP requires many times of calculations until one gets a convergent result especially for a multi-dimensional case like this. However, we notice that a small $O(\mathbf{x}) (\simeq 130)$ was already found after a few times of the CCONE calculations. From this result, GP may provide one of the candidates of \mathbf{x} .

On the other hand, a parameter search by GLS has a shortcoming that it is often stuck into to a local minimum of $O(\mathbf{x})$ unless an appropriate initial parameter set is chosen. To avoid this problem, one needs to change the ini-

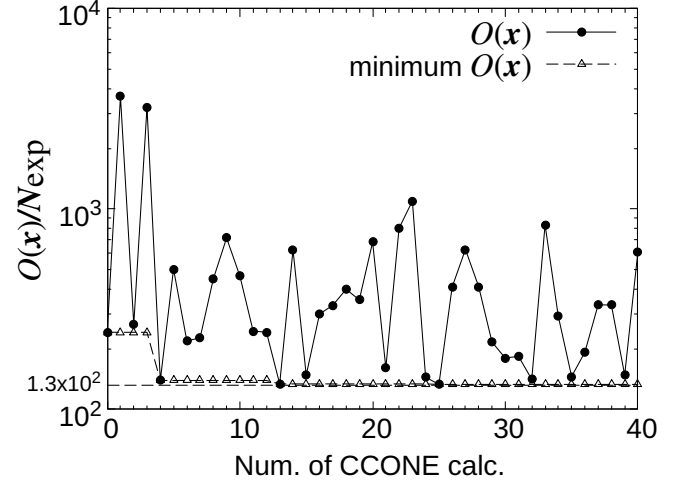


FIG. 3. Objective function normalized to N_{exp} calculated by GP (circle). The x -axis represents the number of CCONE calculation. The minimum $O(\mathbf{x})/N_{\text{exp}}$ in the past calculations is indicated by the triangle.

tial parameter set in several time and check if a consistent result is obtained. However, this procedure also costs a lot of calculations. To overcome this problem, we come up with an idea to combine GP and GLS. A schematic figure is shown in Fig. 4 to illustrate the new approach. The procedure is as follows. We first consider a discrete mesh of the parameter space (a two-dimensional mesh is drawn in Fig. 4; however, actual calculations are carried out in multi-dimensional mesh). We next seek a minimum $O(\mathbf{x})$ on the grids of the mesh within GP, which is shown by the open circle ($\mathbf{x}_{\text{GP}} = [x^{(i)}, x^{(j)}] = [0.2, 0.2]$) in Fig. 4. A real minimum $O(\mathbf{x})$ is expected to be around this grid point and is sought by GLS setting \mathbf{x}_{GP} as an initial parameter set. If this process works well, an expected result would be obtained. In what follows, we call the combination of GP and GLS as GP+GLS.

Figure 5 shows the objective function obtained with the parameter search methods of GLS and GP+GLS. The GP+GLS calculation is launched by using \mathbf{x}_{GP} as explained above. We can see that the objective function of $O(\mathbf{x})/N_{\text{exp}}$ of GP+GLS converges much faster than that of GLS indicated by the closed circle. Furthermore, GP+GLS gives a lower $O(\mathbf{x})/N_{\text{exp}}$ ($\simeq 72$) than that of GP ($\simeq 77$), proving that GP+GLS is more effective than GLS. We depicted 5 δZ_p parameters, which are sensitive to fission fragment yields, at each iteration time of GLS in Fig. 6. Note that the initial values of GP+GLS (iteration time 0) is identical to the result of GP, so that the symbols shown in Fig. 6 is the result after Bayesian optimization with the Gaussian process. As expected, most of δZ_p parameters of GP+GLS does not change significantly at each iteration step. This indicates GP could find δZ_p close to reasonable values. Only δZ_p for $64 \leq A \leq 74$ for GP+GLS shifts from $\delta Z_p \sim -0.5$ at the beginning to $\delta Z_p \sim 0.0$ at the end. This parameter

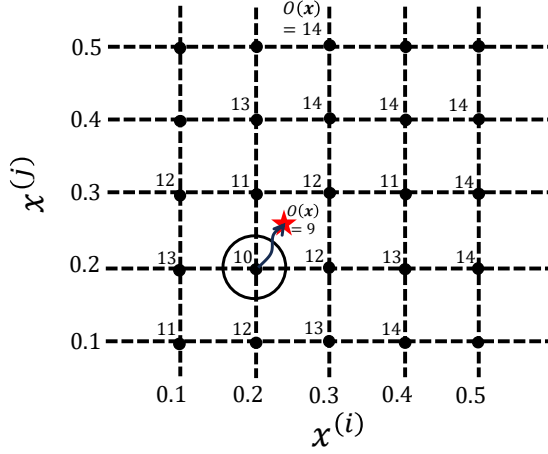


FIG. 4. Schematic figure explaining parameter search by a combination of GP and GLS used in this work. First of all, a multi-dimensional parameter space is discretized by an arbitrary grid size (0.1 in this figure). Then, we seek a minimum $O(\mathbf{x})$ on the grid points by GP. The result is shown by the open circle ($\mathbf{x}_{GP} = [x^{(i)}, x^{(j)}] = [0.2, 0.2]$). Then, a more realistic minimum $O(\mathbf{x})$ shown by a star symbol is sought by GLS setting \mathbf{x}_{GP} as an initial parameter set.

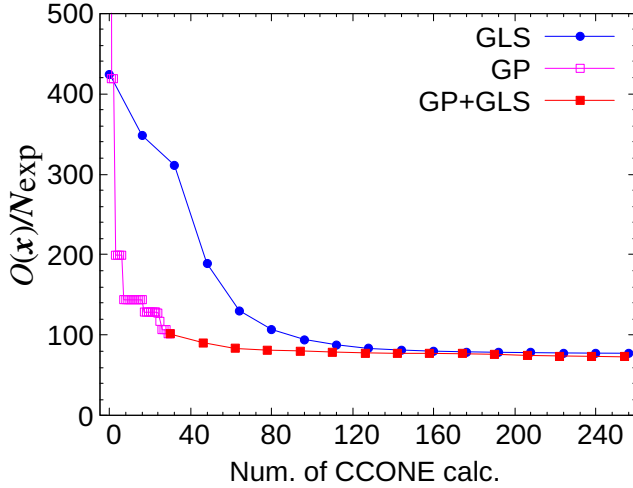


FIG. 5. Objective function normalized to N_{exp} as a function of the number of the CCONE calculation. GP+GLS (solid square) is started from the calculation using the parameter set obtained by GP.

ranges to the far-wing region of fission fragment yields and does not affect the calculated fission observables, namely its sensitivity to the experimental data is limited. In fact, δZ_p for $64 \leq A \leq 74$ as well as $\delta \sigma_p$ has a sensitivity only for 12 PFN experimental data, while other parameters usually have a sensitivity for more than hundred experimental data. It is difficult to determine such a parameter uniquely within the limited number of iteration time by GP. However, this issue is remedied by GLS and the parameters are accommodated to the experimental data more precisely. For the case of GLS, δZ_p

parameters show meaningful changes at first few iterations. After 15 time iteration, the results of GLS become closer to those of GP+GLS, but have some differences leading to the larger objective function as seen in Fig 5. The symmetric part ($108 \leq A \leq 117$) show negative δZ_p , which is consistent to Wahl's evaluation shown in Fig. 2, while the far-wing part ($64 \leq A \leq 74$) is close to zero (GP+GLS) or negative (GP), which contradicts to Wahl's evaluation.

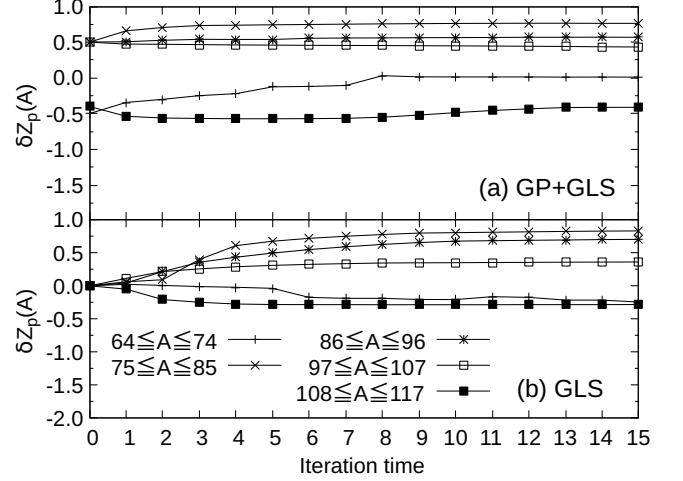


FIG. 6. 5 $Z_p(A)$ parameters at each iteration step of the least square fitting for (a) GP+GLS and (b) GLS.

We plot the correlation matrix of the 15 parameters in Fig 7. Here, the correlation coefficients $\text{COR}(X, Y)$ are defined as $\text{COR}(X, Y) = \frac{\text{COV}(X, Y)}{\sigma(X)\sigma(Y)}$, where $\text{COV}(X, Y)$ are between two variables of X and Y and $\sigma(X)$ are the standard deviations of X . The symbols of $\delta Z_p(i)$ and $\delta \sigma_p(i)$ ($i = 1, \dots, 5$) in Fig. 7 are the corresponding parameters in the mass regions of (1) $64 \leq A \leq 74$, (2) $75 \leq A \leq 85$, (3) $86 \leq A \leq 96$, (4) $97 \leq A \leq 107$, and (5) $108 \leq A \leq 117$. We should note that δZ_p and σ_p in the same mass region have relatively high correlations as is obvious from Eq. (9). Another remarkable point is that $\sigma_p(3)$ and $\sigma_p(4)$ show a relatively strong correlation of about $\text{COR}(X, Y) = -0.54$ despite that they belong to different mass regions. Actually, neighboring mass regions may have a correlation because some fission observables accompany particle emissions, e.g. PFN, decay heats, and delayed neutron yields. In addition, the mass regions of (3) and (4) correspond to $86 \leq A \leq 107$ where fission fragment yields are high, and are sensitive to fission observables. For these reasons, $\sigma_p(3)$ and $\sigma_p(4)$ have a relatively high correlation. However, most pairs of parameters have small correlations and this facts enables us to determine the parameters relatively smoothly.

Next, we compare the calculated fission observables with experimental and evaluated data. The result of independent fission fragment mass yields are shown in Fig 8, where the evaluated data of JENDL-5 [4] are shown

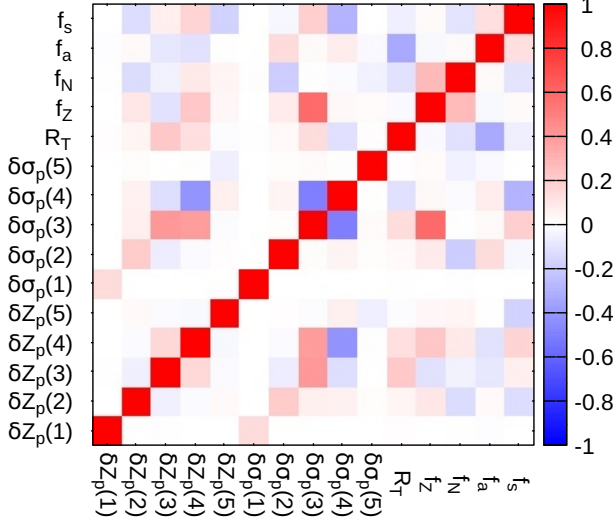


FIG. 7. Correlation matrix of the parameters of $\mathbf{x} = (\{\delta Z_p\}, \{\delta \sigma_p\}, R_T, f_Z, f_N, f_a, f_s)$.

together. The results of GP, GP+GLS, and JENDL-5 show a good agreement to each other. However, both GP and GLS provide higher yields than JENDL-5 in the mass region from $92 \leq A \leq 98$. This difference must be compensated because independent fission fragment mass yields are normalized to 2. Actually, the fragment distributions of GP and GLS are slightly narrower than JENDL-5. Figure 9 illustrates the result of IFY of fragments. The experimental data of Rudstam [31] are also shown for comparison. Despite that we reduced the number of adjustable parameters for $\delta Z_p(A)$ and $\delta \sigma_p(A)$, both the calculated result of GP and GP+GLS reproduce the experimental data reasonably.

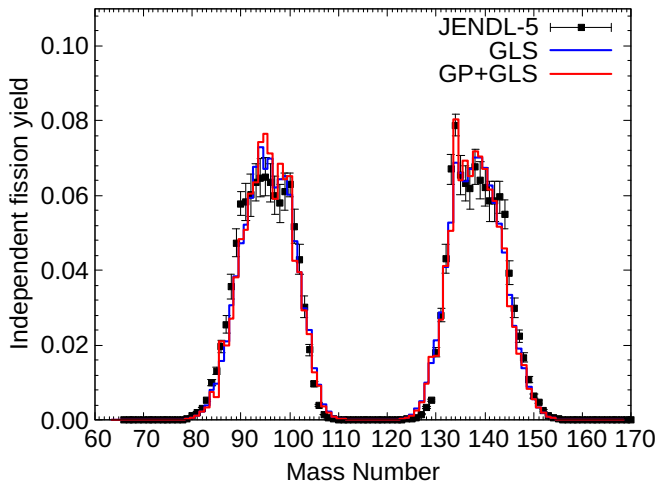


FIG. 8. Independent fission mass yields calculated with the parameter search methods of GP and GP+GLS. The evaluated data of JENDL-5 are also shown.

Figure 10 compares the number of prompt neutron multiplicity as a function of fission fragment mass. The experimental data exhibit the so-called saw-tooth structure, namely the numbers of prompt-neutron increase from $A = 70$ to 110 in light fragments, and sudden decrease when jumping to heavy fragments, but again increase from $A = 120$ to 160. Although the calculated result successfully reproduces the experimental data, especially those of Nishio et al. [33]. In Fig. 11, the results of (a) β -ray and (b) γ -ray decay heats and (c) delayed neutron yields as a function of time after an instant neutron irradiation are shown. The decay heats of β - and γ -rays are reproduced well. On the other hand, the result of delayed neutron yields is not reproduced well both for GLS and GP+GLS. Delayed neutron yields are rather sensitive to the charge distribution [45] and we confirmed that the 5 parameters of δZ_p and σ_p are not enough to reproduce the experimental data.

B. Full parameter set for $\delta Z_p(A)$ and $\delta \sigma_p(A)$

Now we demonstrate the result of full 54 parameter set for $\delta Z_p(A)$ and $\delta \sigma_p(A)$, namely 113 parameters in total. We first discuss the result of objective function normalized to N_{exp} at each iteration step. The result is shown in Fig. 12. As in the case of 5 parameters for $\delta Z_p(A)$ and $\delta \sigma_p(A)$, GP+GLS starts with the parameter set obtained after 30 iterations of GP. The objective function of GP+GLS decreases more quickly than that of GP and converges to $O(\mathbf{x})/N_{\text{exp}} \sim 44$, while the objective function of GLS converges to $O(\mathbf{x})/N_{\text{exp}} \sim 46$. Thus, it can be concluded that GP+GLS can find a better result than GLS even when the number of free parameter increases. Hereafter, we only show the results of GP+GLS regarding that its performance is better than those of GLS. We compare $\delta Z_p(A)$ and $\sigma_p(A)$ obtained by the parameter search and Wahl's evaluation in Fig. 13. Note that a part of the far-wing regions, which are $64 \leq A \leq 69$ and $169 \leq A \leq 174$, is excluded from the parameter search target because they are insensitive to any of the experimental data listed in Table I and cannot be adjusted by the GLS. The calculated result has a staggering distribution, but the average behavior shows a similar trend to Wahl's evaluation. It is interesting that the saw-tooth structures evaluated by Wahl around $A = 110$ and 126 are also confirmed by the present parameter search method as well. On the other hand, $Z_p(A)$ at $70 \leq A \leq 75$ ($163 \leq A \leq 168$) are close to zero for the present result, showing a difference from the Wahl's evaluation. As for $\sigma_p(A)$, the present result shows a completely different result from the Wahl's evaluation. For $70 \leq A \leq 86$, $\sigma_p(A)$ are almost equal to 0.5 and they become < 0.5 with some staggering behavior for $86 \leq A \leq 110$. These structure may arise from the shell structure of nuclei at fissioning point. A increase as estimated by Wahl from $A = 75$ to 104 and a plateau around the symmetric region are not obtained for the

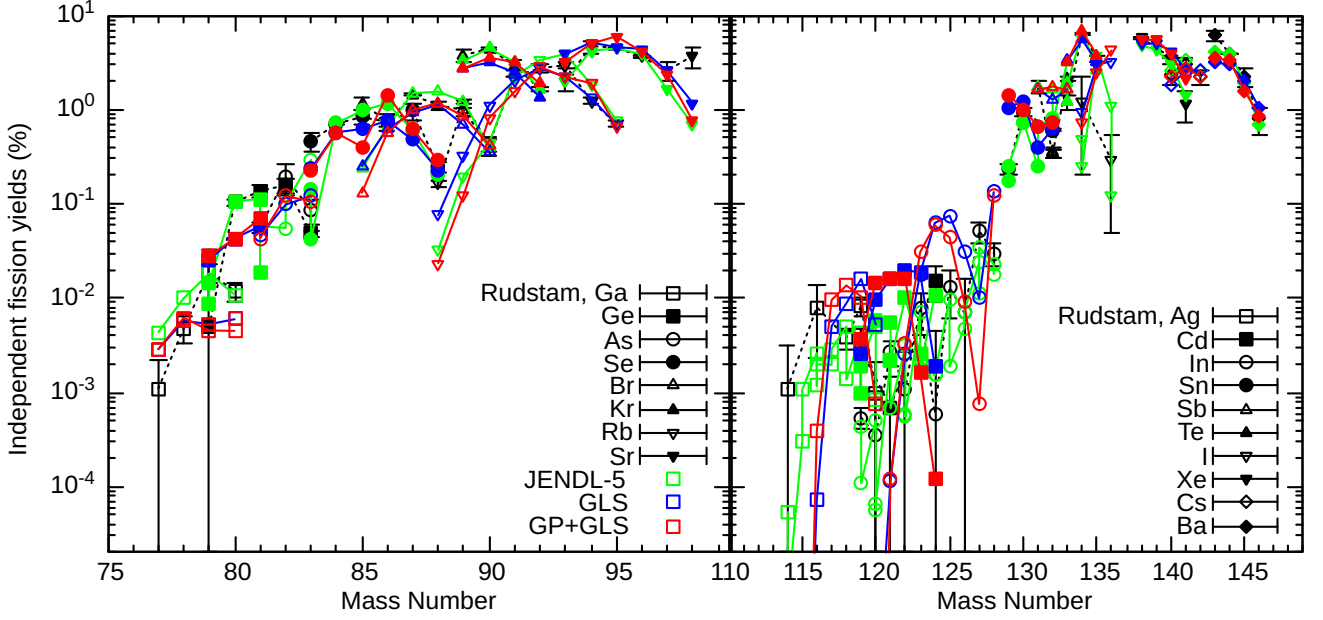
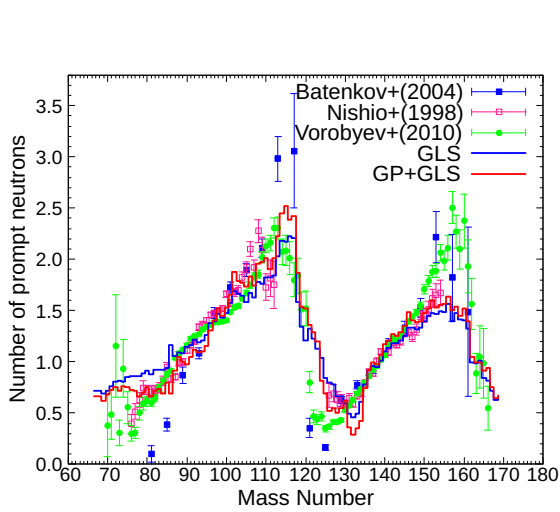
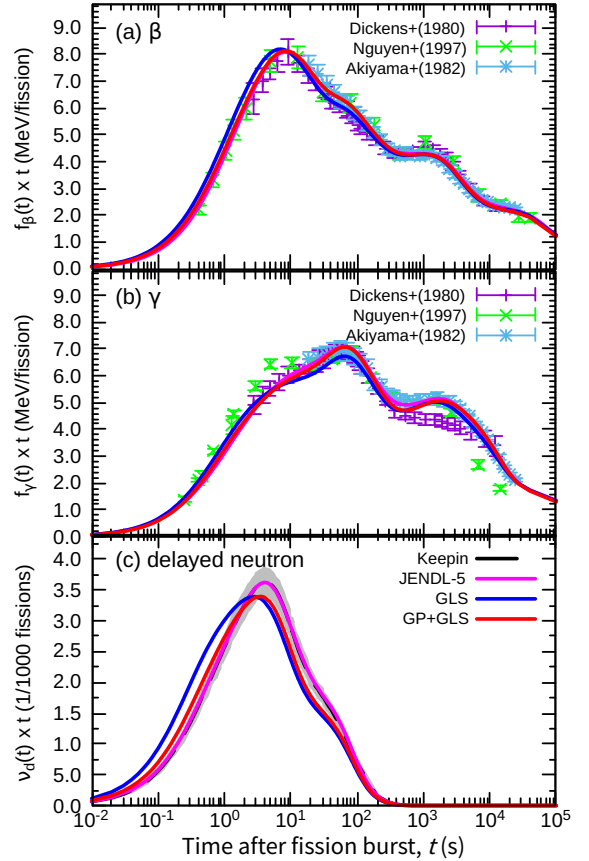


FIG. 9. Independent fission fragment yields.

FIG. 10. Number of prompt neutron multiplicity as a function of fission fragment mass in case of 5 parameters for δZ_p and $\delta\sigma_p$.

present model.

Figure 14 shows the independent fission mass yields. One of the remarks of the GP+GLS result is that it shows a peak at $A = 141$, which was not observed for JENDL-5. The peak is mainly due to IFY of ^{141}Cs , which is 4.9% for GP+GLS and 3.3% for JENDL-5. From the analysis, the pre-neutron fission fragment yield of ^{142}Cs is about 4.9% in the present calculation (about 3.4% for ^{141}Cs). The high pre-neutron fission fragment yield of ^{142}Cs is attributed from $Z_p(A) = 55.044$ after the parameter fitting. As a result, the feeding to ^{141}Cs by 1-neutron emission works effectively to make the peak. We

FIG. 11. (a) β -ray and (b) γ -ray decay heats and (c) delayed neutron yields as a function of time after fission burst (instant neutron radiation). The evaluated result of JENDL-5 (magenta) is also shown together.

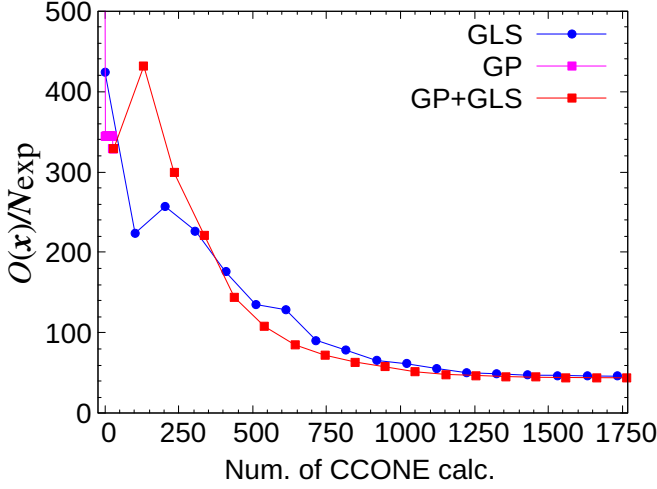


FIG. 12. Objective function textcolorrednormalized to N_{exp} and the required number of CCONE calculation.

also see that the independent fission mass yields for light fragments for $90 \leq A \leq 95$ are slightly larger than those for JENDL-5. This was already found in Fig. 8 and was also confirmed in other work of Ref. [9] that adopts the Hauser-Feshbach statistical model to calculate independent fission mass yields from pre-neutron fission yields. Since JENDL-5 did not take into account the effects of TKE and PFN and these correlations in its evaluated fission yield data [46], this may trigger the deviations of independent fission mass yields around the peak of light fragments. Figure 15 shows the calculated IFY together with experimental data [31]. Since the number of free parameters increases, we can observe some improvements comparing with Fig. 8, for example, in Rb, Ag and In isotopes. The present result of GP+GLS is comparable to the evaluated data of JENDL-5; however, we obtained some improvements for Ga, Rb, and In isotopes. We also noticed underestimations of GP+GLS for Ba isotopes; however the cumulative yields of those nuclei are not deficient from the experimental data. For example, the present results of ^{144}Ba and ^{145}Ba are 4.20% and 1.38%, respectively, while the experimental data are $4.40 \pm 0.66\%$ and $1.90 \pm 0.32\%$ [32], respectively.

Figure 16 is the result of the number of prompt neutron multiplicity as a function of fragment mass. The saw-tooth structure observed in experimental data is nicely reproduced as we already observed in Fig. 10. The total number of prompt fission neutrons was $\nu_p = 2.378$ for the case of 5 parameters for $Z_p(A)$ and $\sigma_p(A)$, while in this case we obtain $\nu_p = 2.407$ which is in a good agreement with experimental data and the JENDL-5 evaluation ($\nu_p = 2.413$).

Figure 17 shows the decay heats of γ - and β -rays and delayed neutron yields. The result of β -ray decay heats are slightly larger than the experimental data of Nguyen et al. [42] at $0.4 \leq t \leq 5.0$ s, while it is close to JENDL-5 and nicely reproduces the experimental data after $t = 5.0$

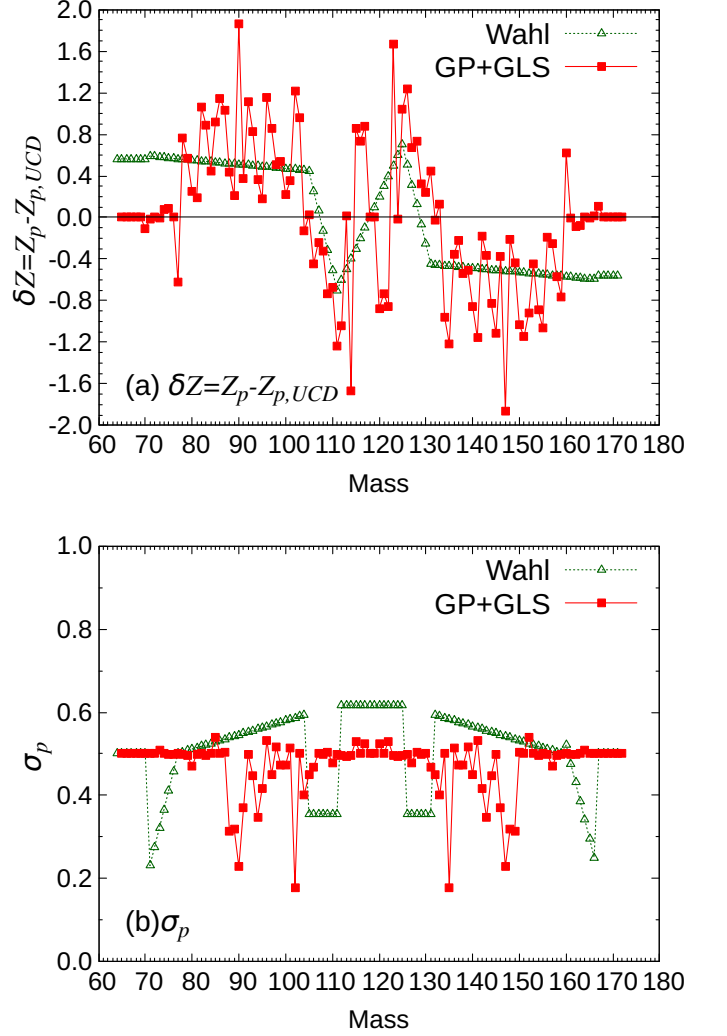


FIG. 13. (a) Difference between unchanged charge distribution and evaluated value of the most probable proton number Z_p . The calculated results of GP+GLS are compared with the evaluated data of Wahl [18]. (b) Width parameters of charge distributions.

s. Here, t represents time after fission burst shown as x -axis in Fig. 17. The result of γ -ray decay heat is closer than JENDL-5 to the experimental data of Nguyen et al. [42] at $0.25 \leq t \leq 2.00$ s. Since we have only 1 data set at the early stage ($t \leq 2$ s) after fission burst, we are not still sure which data of the present work or JENDL-5 are more reliable both for β - and γ -decay heats, and experimental researches are thus required in this respect. Above $t = 2$ s, both GP+GLS and JENDL-5 show a good agreement with experimental data of Akiyama et al. [41]. Note that the data of Akiyama et al. [41] are those for fast neutron fission; however, we expect the result does not differ so much from thermal-neutron induced fission. Next, we discuss the result of delayed neutron yields shown in Fig. 17(c). Comparing the result for the 5 parameters for $\delta Z_p(A)$ and $\delta \sigma_p(A)$ in Fig. 11,

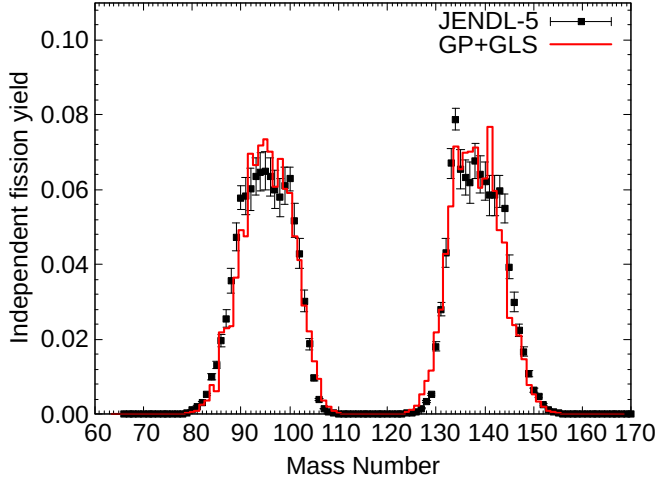


FIG. 14. Independent fission mass yields for full parameter set for $\delta Z_p(A)$ and $\delta\sigma_p(A)$.

the calculated delayed neutron yields are drastically improved and comparable to the evaluated data of JENDL-5. So, the parameter search with enough number of free $\delta Z_p(A)$ and $\delta\sigma_p(A)$ is important. The number of total delayed neutron yields is about $\nu_d = 0.01595$ for GP+GLS, which reasonably reproduces the experimental data of Keepin et al. [44] ($\nu_d = 0.0158 \pm 0.0005$).

V. SUMMARY

We calculated fission fragment yields of the thermal-neutron induced fission of ^{236}U and relevant fission observables with a newly developed CCONE system. To determine parameters involved in this system, a combination of a Gaussian process and a least square fitting was introduced. At first, we demonstrated the performance of parameter search method of GLS and GP+GLS. It was found that the GP+GLS method successfully found the most likely parameter set and was suitable for the present purpose as like involving a lot

of parameters exceeding 100. We have shown that fission observables such as prompt fission neutrons, decay heats, and delayed-neutrons were reproduced in a comparable level to JENDL-5. The total number of prompt neutrons and delayed neutrons were also reasonably reproduced. This fact indicates that the present approach has a potential to apply a practical evaluation of fission fragment yields.

We still have a few questions arising from this work. We could reproduce the overall structure of experimental data with only 5 parameters for $\delta Z_p(A)$ and $\delta\sigma_p(A)$ except delayed neutrons. This means that we may have a possibility to reproduce experimental data with less number of parameters than 54 for them. If it is true, an evaluation of fission fragment yields with this framework becomes more effective because we can reduce the computational time. In addition, we observed that a staggering structure in $\delta Z_p(A)$ and $\delta\sigma_p(A)$ in Fig. 13, which was not found in the Wahl's evaluation. It will be interesting to confirm this structure within a microscopic framework.

Our future perspective is to apply this framework to study different fission systems. Now we calculate thermal-neutron induced fission of ^{233}U and ^{239}Pu . We also plan to open the present result in the ENDF-6 format or other modern format to online so that anyone can access. In this case, covariance data will be also provided as done in JENDL-5.

ACKNOWLEDGEMENTS

The authors thank Dr. S. Okumura at IAEA and Dr. T. Kawano at LANL for useful comments. They also thank Research Coordinated Program. FM acknowledges a special support from Dr. S. Yoshida at Utsunomiya university. This work is supported by JSPS KAKENHI Grant Number 21H01856 and MEXT Innovative Nuclear Research and Development Program "Fission product yields predicted by machine learning technique at unmeasured energies and its influence on reactor physics assessment" entrusted to the Tokyo Institute of Technology.

-
- [1] Bernstein A, Bowden N, Goldblum BL, et al. Colloquium: Neutrino detectors as tools for nuclear security. *Rev Mod Phys.* 2020 Mar;92:011003. Available from: <https://link.aps.org/doi/10.1103/RevModPhys.92.011003>.
 - [2] Pritychenko B, Oberstedt S, Cabellos O, et al. Summary report of the 1st rcm of the crp on the updating fission yield data for applications. 2021 4; Available from: <https://www.osti.gov/biblio/1807955>.
 - [3] Shibata K, Iwamoto O, Nakagawa T, et al. Jendl-4.0: A new library for nuclear science and engineering. <https://doi.org/10.1080/1881124820119711675>. 2012; 48:1–30. Available from: <https://www.tandfonline.com/doi/abs/10.1080/18811248.2011.9711675>.
 - [4] Iwamoto O, Iwamoto N, Kunieda S, et al. Japanese evaluated nuclear data library version 5: Jendl-5. *Journal of Nuclear Science and Technology.* 2023;60(1):1–60. Available from: <https://doi.org/10.1080/00223131.2022.2141903>.
 - [5] Huang Y, Feng Y, Xiao E, et al. Influence of pre-scission neutron emission on high-energy ^{238}U fission studied by the langevin approach. *Phys Rev C.* 2022 Nov; 106:054606. Available from: <https://link.aps.org/doi/10.1103/PhysRevC.106.054606>.
 - [6] Tanaka S, Nishimura N, Minato F, et al. Postfission properties of uranium isotopes: A hybrid method with

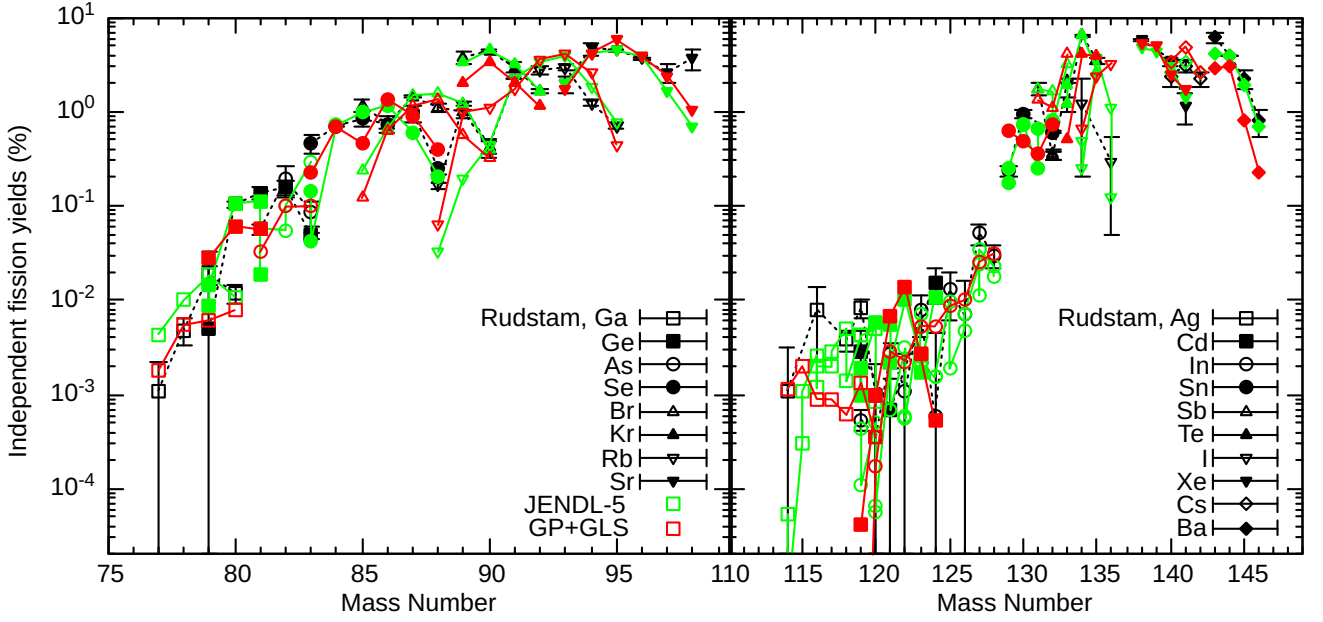


FIG. 15. Same as Fig. 8, but for full parameter set for $\delta Z_p(A)$ and $\delta \sigma_p(A)$.

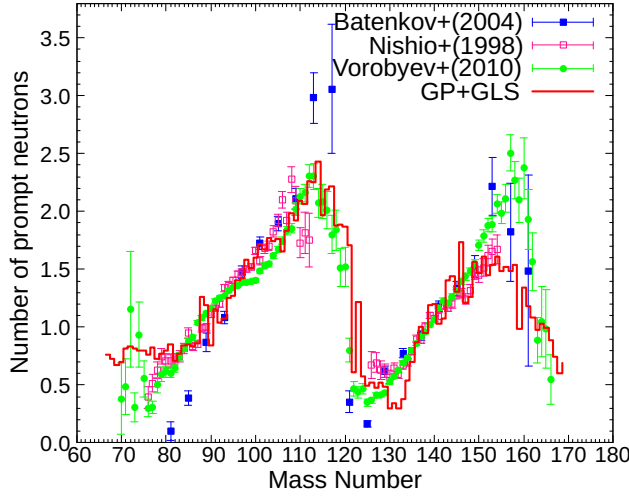


FIG. 16. Number of prompt neutron multiplicity as a function of fission fragment mass in case of full parameter set for δZ_p and $\delta \sigma_p$.

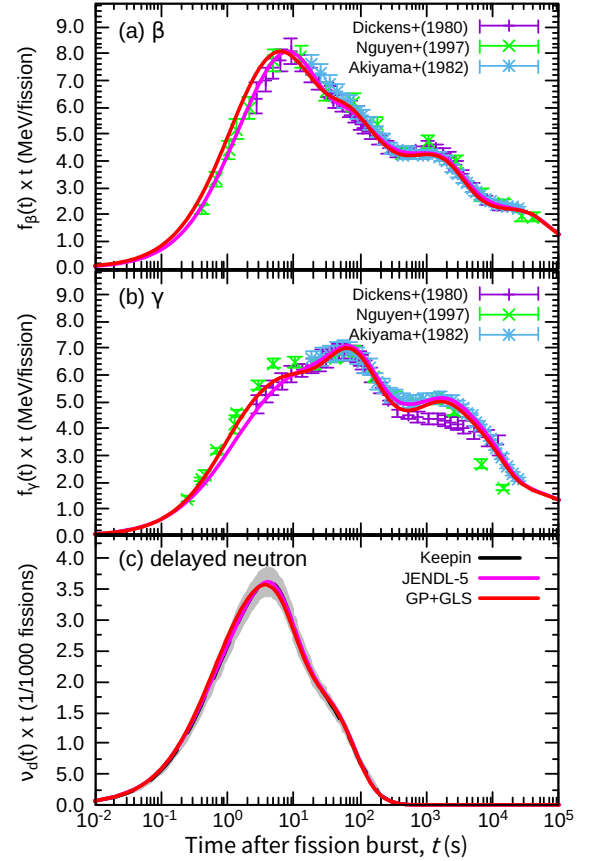


FIG. 17. Same as Fig. 11, but for full parameter set for $\delta Z_p(A)$ and $\delta \sigma_p(A)$.

langevin dynamics and the hauser-feshbach statistical model. Phys Rev C. 2023 Nov;108:054607. Available from: <https://link.aps.org/doi/10.1103/PhysRevC.108.054607>.

- [7] Fujio K, Okumura S, Ishizuka C, et al. Connection of four-dimensional langevin model and hauser-feshbach theory to describe statistical decay of fission fragments. Journal of Nuclear Science and Technology. 2023; 0(0):1–14. Available from: <https://doi.org/10.1080/00223131.2023.2273470>.

- [8] Iwamoto O, Iwamoto N, Kunieda S, et al. The CCONE Code System and its Application to Nuclear Data Evaluation for Fission and Other Reactions. Nuclear Data

- Sheets. 2016 1;131:259–288.
- [9] Okumura S, Kawano T, Jaffke P, et al. $^{235}\text{U}(\text{n},\text{f})$ Independent fission product yield and isomeric ratio calculated with the statistical Hauser-Feshbach theory. *Journal of Nuclear Science and Technology*. 2018;55(9):1009–1023. Available from: <https://doi.org/10.1080/00223131.2018.1467288>.
 - [10] Lovell AE, Kawano T, Okumura S, et al. Extension of the Hauser-Feshbach fission fragment decay model to multichance fission. *Phys Rev C*. 2021 Jan;103:014615. Available from: <https://link.aps.org/doi/10.1103/PhysRevC.103.014615>.
 - [11] Okumura S, Kawano T, Lovell AE, et al. Energy dependent calculations of fission product, prompt, and delayed neutron yields for neutron induced fission on ^{235}U , ^{238}U , and ^{239}Pu . *J of Nucl Sci Technol*. 2021;59:96–109.
 - [12] Litaize O, Serot O, Berge L. Fission modelling with firelin. *The European Physical Journal A*. 2015; 51:177. Available from: <https://doi.org/10.1140/epja/i2015-15177-9>.
 - [13] Piau V, Litaize O, Chebboubi A, et al. Neutron and gamma multiplicities calculated in the consistent framework of the hauser-feshbach monte carlo code firelin. *Physics Letters B*. 2023;837:137648. Available from: <https://www.sciencedirect.com/science/article/pii/S0370269322007821>.
 - [14] Verbeke J, Randrup J, Vogt R. Fission reaction event yield algorithm, freya — for event-by-event simulation of fission. *Computer Physics Communications*. 2015;191:178–202. Available from: <https://www.sciencedirect.com/science/article/pii/S0010465515000466>.
 - [15] Verbeke J, Randrup J, Vogt R. Fission reaction event yield algorithm freya 2.0.2. *Computer Physics Communications*. 2018;222:263–266. Available from: <https://www.sciencedirect.com/science/article/pii/S001046551730293X>.
 - [16] Iwamoto O. Development of a Comprehensive Code for Nuclear Data Evaluation, CCONE, and Validation Using Neutron-Induced Cross Sections for Uranium Isotopes. *Journal of Nuclear Science and Technology*. 2007; 44(5):687–697.
 - [17] Oyamatsu K. Easy-to-use application programs to calculate aggregate fission-product properties on personal computers. In: *Proc. 1998 Symposium on Nuclear Data, Nov. 1998, JAERI, Tokai, Japan, JAERI-Conf 99-002*; 1999. p. 234–239.
 - [18] Wahl A. Systematics of fission-product yields. Los Alamos National Laboratory; 2002. LA-13928.
 - [19] Kawano T, Talou P, Stetcu I, et al. Statistical and evaporation models for the neutron emission energy spectrum in the center-of-mass system from fission fragments. *Nuclear Physics A*. 2013;913:51–70. Available from: <https://www.sciencedirect.com/science/article/pii/S0375947413005952>.
 - [20] Meadows J, Budtz-Jorgensen C. The fission fragment angular distributions and total kinetic energies for $^{235}\text{u}(\text{n},\text{f})$ from .18 to 8.83 mev. Argonne National Laboratory; 1982. ANL/NDM-64.
 - [21] Madland D. Total prompt energy release in the neutron-induced fission of ^{235}u , ^{238}u , and ^{239}pu . *Nuclear Physics A*. 2006;772(3):113–137. Available from: <https://www.sciencedirect.com/science/article/pii/S0375947406001503>.
 - [22] D D. Fision fragment mass distributions and total kinetic energy release of $^{235}\text{-uranium}$ and $^{238}\text{-uranium}$ in neutron-induced fission at intermediate and fast neutron energies [ph.d thesis] [dissertation]. Colorado State University; 2014.
 - [23] England T, Rider B. Evaluation and Compilation of Fission Product Yields. Los Alamos National Laboratory; 1994. LA-UR-94-3106.
 - [24] Mengoni A, Nakajima Y. Fermi-Gas Model Parametrization of Nuclear Level Density. *Journal of Nuclear Science and Technology*. 1994;31(2):151–162.
 - [25] Gilbert A, Cameron AGW. A composite nuclear-level density formula with shell corrections. *Can J Phys*. 1965; 43:1446–1496.
 - [26] Koning A, Delaroche J. Local and global nucleon optical models from 1 kev to 200 mev. *Nuclear Physics*. 2003; A713:231.
 - [27] Capote R, Herman M, Obložinský P, et al. Ripl – reference input parameter library for calculation of nuclear reactions and nuclear data evaluations. *Nuclear Data Sheets*. 2009 12;110:3107–3214.
 - [28] Kopecky J, Uhl M. Test of gamma-ray strength functions in nuclear reaction model calculations. *Phys Rev C*. 1990 May;41:1941–1955. Available from: <https://link.aps.org/doi/10.1103/PhysRevC.41.1941>.
 - [29] Huang W, Wang M, Kondev F, et al. The AME 2020 atomic mass evaluation (i). evaluation of input data, and adjustment procedures*. *Chinese Physics C*. 2021 mar;45(3):030002. Available from: <https://doi.org/10.1088/1674-1137/abddb0>.
 - [30] Watanabe S, Minato F, Kimura M, et al. Nuclear data generation by machine learning (I) application to angular distributions for nucleon-nucleus scattering. *Journal of Nuclear Science and Technology*. 2022;59(11):1399–1406. Available from: <https://doi.org/10.1080/00223131.2022.2061622>.
 - [31] Rudstam G, Johansson PI, Tengblad O, et al. Beta and Gamma Spectra of Short-Lived Fission Products. *Atomic Data and Nuclear Data Tables*. 1990 Jan;45:239.
 - [32] Tipnis SV, Campbell JM, Couchell GP, et al. Yields of short-lived fission products produced following $^{235}\text{U}(\text{n}_{\text{th}},\text{f})$. *Phys Rev C*. 1998 Aug;58:905–915. Available from: <https://link.aps.org/doi/10.1103/PhysRevC.58.905>.
 - [33] Nishio K, Nakagome Y, Yamamoto H, et al. Multiplicity and energy of neutrons from $^{235}\text{U}(\text{n}_{\text{th}},\text{f})$ fission fragments. *Nuclear Physics A*. 1998 mar;632(4):540–558.
 - [34] Batenkov OA, Boykov GA, Hamsch FJ, et al. Prompt Neutron Emission in the Neutron-Induced Fission of ^{239}Pu and ^{235}U . *AIP Conf Proc*. 2005;769(1):1003.
 - [35] Vorobyev AS, Shcherbakov OA, Gagarski AM, et al. Investigation of the prompt neutron emission mechanism in low energy fission of $^{235,233}\text{U}(\text{n}_{\text{th}},\text{f})$ and $^{252}\text{Cf}(\text{sf})$. In: *European Physical Journal Web of Conferences*; (European Physical Journal Web of Conferences; Vol. 8); Oct.; 2010. p. 03004.
 - [36] Boldeman J, de L Musgrove A, Walsh R. Prompt neutrons from ^{236}u fission fragments. *Australian Journal of Physics*. 1971;24:821–834. Available from: <https://doi.org/10.1071/PH710821>.
 - [37] Fraser JS, Milton JCD. Nuclear fission. *Annual Review of Nuclear Science*. 1966;16(1):379–444. Available from: <https://doi.org/10.1146/annurev.ns.16.120166.002115>.

- [38] Maslin EE, Rodgers AL, Core WGF. Prompt neutron emission from u^{235} fission fragments. *Phys Rev.* 1967 Dec; 164:1520–1527. Available from: <https://link.aps.org/doi/10.1103/PhysRev.164.1520>.
- [39] Göök A, Hambsch FJ, Oberstedt S, et al. Prompt neutrons in correlation with fission fragments from $^{235}\text{U}(n, f)$. *Phys Rev C.* 2018 Oct;98:044615. Available from: <https://link.aps.org/doi/10.1103/PhysRevC.98.044615>.
- [40] Pleasonton F, Ferguson RL, Schmitt HW. Prompt gamma rays emitted in the thermal-neutron-induced fission of ^{235}U . *Phys Rev C.* 1972 Sep;6:1023–1039. Available from: <https://link.aps.org/doi/10.1103/PhysRevC.6.1023>.
- [41] Akiyama M, An S. Measurement of fission product decay heat for fast reactor. In: *Proc. of Int. Conf. on Nucl. Data for Science and Technol.*; 1982. p. 237. Antwerp, Belgium.
- [42] Decay Heat Measurements Following Neutron Fission of ^{235}U and ^{239}Pu ; 1997.
- [43] Dickens J, Love TA, McConnell JW, et al. Fission Product Energy Release for Time following Thermal Neutron Fission of ^{235}U between 2 and 14,000 seconds. *Nucl Sci Eng.* 1980;74:106–129.
- [44] Keepin G, Wimett T, Zeigler R. Delayed neutrons from fissionable isotopes of uranium, plutonium and thorium. *Journal of Nuclear Energy.* 1957;6(1):IN2 – 21. Available from: <http://www.sciencedirect.com/science/article/pii/089139195790178X>.
- [45] F M. Neutron energy dependence of delayed neutron yields and its assessments. *J Nucl Sci Technol.* 2018; 55:1054–1064.
- [46] Tsubakihara K, Okumura S, Ishizuka C, et al. Evaluation of fission product yields and associated covariance matrices. *Journal of Nuclear Science and Technology.* 2021;58(2):151–165. Available from: <https://doi.org/10.1080/00223131.2020.1813643>.